Sub-microsecond pulsed atmospheric glow discharges with and without dielectric barrier

Shutong Song, Ying Guo, Wonho Choe, Jie Zhang, Jing Zhang et al.

Citation: Phys. Plasmas **19**, 123508 (2012); doi: 10.1063/1.4772780
View online: http://dx.doi.org/10.1063/1.4772780
View Table of Contents: http://pop.aip.org/resource/1/PHPAEN/v19/i12
Published by the American Institute of Physics.

Sub-microsecond pulsed atmospheric glow discharges with and without dielectric barrier

Shutong Song,[1] Ying Guo,[1,2] Wonho Choe,[3] Jie Zhang,[1,2] Jing Zhang,[1,2] and J. J. Shi[1,2,a)]
[1]College of Science, Donghua University, Shanghai 201620, People's Republic of China
[2]Member of Magnetic Confinement Fusion Research Center, Ministry of Education of the People's Republic of China, Shanghai 201620, People's Republic of China
[3]Department of Physics, Korea Advanced Institute of Science and Technology, 291 Daehak-ro, Yuseong-gu, Daejeon 305-701, South Korea

(Received 18 September 2012; accepted 3 December 2012; published online 20 December 2012)

The discharge characteristics and mechanism of glow discharges in atmospheric pressure helium excited by repetitive voltage pulses with and without dielectric barriers are numerically studied using a one-dimensional self-consistent fluid model. The waveforms of discharge current density show that one discharge event occurs during the voltage pulse with bare electrodes and two distinct discharge events happen at the rising and falling phases of voltage pulse with dielectric barrier electrodes, respectively. The spatial profiles of electron and electric field at the time instant of discharge current peak reveal that the electrons are trapped in the plasma bulk with bare electrodes, while the electrons are accumulated in the region between the sheath and plasma bulk with dielectric barrier electrodes. Furthermore, the spatio-temporal evolution of electron density and mean electron energy clearly demonstrate the dynamics of discharge ignition, especially the temporal evolution of sheath above the instantaneous cathode. © *2012 American Institute of Physics*. [http://dx.doi.org/10.1063/1.4772780]

I. INTRODUCTION

In the past decades, the atmospheric pressure dielectric barrier discharges (DBDs) are studied intensively for their wide application scopes,[1] such as etching, surface modification, deposition of functionalized film,[2,3] and biological manipulation.[4] Traditionally, atmospheric pressure DBDs are driven by the sinusoidal voltage with repetition frequencies of kilohertz to megahertz.[5,6] Recently, atmospheric pressure glow discharges (APGDs) excited by sub-microsecond voltage pulses have drawn much attention for their higher efficiency of power consumption and electron generation than that of conventional non-pulse DBDs.[7] Furthermore, the sub-microsecond pulse voltage can ignite the homogeneous APGDs without the dielectric barriers at the repetition frequency range of kilohertz,[7,8] even in ambient air,[9,10] which opens the wider potential application of nonthermal processing, such as food decontamination[11] and industrial surface treatment.[12] It was found that in pulsed APGDs with bare electrodes, one discharge event occurred at the falling phase of voltage pulse[8,13] and there were two discharge events happened with dielectric insulated electrodes at the rising and falling phase of voltage pulse.[13,14] By extending the duration of voltage pulses, the discharge events with multiple current peaks were observed,[15] which is comparable with that of conventional DBDs.[5] The discharge electrical characteristics of sub-microsecond pulsed atmospheric glow discharges without dielectric barrier were studied computationally and experimentally, which suggested that the discharge was initiated by Townsend discharge and the ignition was delayed with respect to the applied voltage.[16] Despite significant interest of achieving the APGDs excited by the pulse voltage under sub-microsecond with high stability and reactivity, their underlying physics in terms of discharge dynamics and mechanism remains incomplete. Here, a one-dimensional self-consistent fluid model was developed to investigate the discharge characteristics and mechanism in terms of current voltage characteristics and spatio-temporal evolution of plasma species, electric field and mean electron energy.

II. MODEL DESCRIPTION

The numerical model considers the parallel-plate configuration with the discharge gap distance of 2 mm. The ceramic sheets with 1 mm in thickness and the relative permittivity of 9.0 are introduced as the dielectric barriers.

Table I gives the elementary reactions in helium with five plasma species of electrons (e), metastable helium atom (He*), metastable helium molecule (He_2*), helium ion (He^+), and molecular helium ion (He_2^+), in which the reaction rate coefficients and transport coefficients follow the data in the literature.[17]

The governing equations in the model include the continuity equation of plasma species with the drift-diffusion approximation, the electron energy conservation equation and Poisson's equation as follows[15]:

$$\frac{\partial n_i}{\partial t} + \nabla \cdot \mathbf{\Gamma}_i = S_i, \quad \mathbf{\Gamma}_i = \mathrm{sgn}\,(q_i) n_i \mu_i \mathbf{E} - D_i \nabla n_i, \tag{1}$$

$$\frac{\partial n_e \varepsilon}{\partial t} + \nabla \cdot \left(\frac{5}{3} \varepsilon \mathbf{\Gamma}_e - \frac{5}{3} n_e D_e \nabla \varepsilon \right) = -e \mathbf{\Gamma}_e \cdot \mathbf{E} - \sum_j \Delta E_j K_j - 3 \frac{m_e}{m_{He}} K_{el} k_b (T_e - T_{He}), \tag{2}$$

$$\varepsilon_0 \nabla \cdot \mathbf{E} = \sum_i q_i n_i. \tag{3}$$

a)Author to whom correspondence should be addressed. Electronic mail: JShi@dhu.edu.cn.

TABLE I. Elementary reactions and their reaction rates, energy loss due to the inelastic collision. T_e is in eV.

Reactions	Rate coefficients	ΔE (eV)
He+e = He*+e	$2.308 \times 10^{-10} T_e^{0.31} \exp\left(-\frac{2.297\times10^5}{T_e}\right)$ (cm^3/s)	19.8
He+e = He^++ 2e	$2.584 \times 10^{-12} T_e^{0.68} \exp\left(-\frac{2.854092\times10^5}{T_e}\right)$ (cm^3/s)	24.6
He*+e = He^++ 2e	$4.661 \times 10^{-10} T_e^{0.6} \exp\left(-\frac{5.546\times10^4}{T_e}\right)$ (cm^3/s)	4.87
He_2^++e = He*+He	$5.386 \times 10^{-7} T_e^{-0.5}$ (cm^3/s)	
He^++2He = He_2^++He	1.1×10^{-31} (cm^6/s)	
He*+2He = He_2*+He	1.3×10^{-33} (cm^6/s)	
He*+e = He+e	$1.099 \times 10^{-11} T_e^{0.31}$ (cm^3/s)	−19.8
He_2*+e = He_2^++2e	$1.268 \times 10^{-12} T_e^{0.71} \exp\left(-\frac{3.945\times10^4}{T_e}\right)$ (cm^3/s)	3.4
He*+He* = He^++He+e	2.7×10^{-10} (cm^3/s)	−15

where the subscripts i, e and He indicate the ith species, electrons and background helium gas, respectively. n is the number density, Γ is the flux in the drift-diffusion approximation, S is the net creation rate, μ and D are the coefficients of mobility and diffusion, E and ε are the electric field and the mean electron energy. ΔE_j and K_j are energy loss and rate coefficient of reaction j, K_{el} is momentum transfer rate between electrons and background helium. m_e and m_{He} are the masses of electron and helium, k_b, T_e and T_{He} are the Boltzmann constant, electron temperature and background helium gas temperature, q and ε_0 are the elementary charge and vacuum permittivity, respectively. The gas temperature of T_{He} is fixed at 300 K.

Boundary condition of electron is determined by the electron flux, which is given by the sum of thermal flux and secondary emission flux. The energy of secondary emitted electron is fixed at 1 eV and the secondary electron emission coefficient is assumed to be 0.02. The ions are assumed to be mobility limited at the boundaries and their boundary fluxes are given by the sum of the mobility and thermal fluxes. The boundary fluxes of metastables are assumed to be thermally limited.

III. RESULTS AND DISCUSSIONS

Figure 1(a) presents the waveforms of applied pulse voltage and discharge current density with the bare electrodes. The applied unipolar voltage pulse has the pulse duration of 400 ns, the rising and falling duration of 100 ns, respectively, with the amplitude of 600 V and the repetition frequency of 10 kHz. The discharge current density grows during the applied voltage pulse and reaches its amplitude of 0.20 A/m^2 at the time instant of 600 ns, which corresponds to the time instant of voltage going down. On the other hand, Figure 1(b) gives the waveforms of applied pulse voltage and discharge current density with the dielectric barrier electrodes. The time scales of voltage pulse in terms of the rising duration, falling duration and pulse duration are the same as that in Fig. 1(a). Since it is important to compare the discharge characteristics and mechanism of APGDs excited by the voltage pulses at the same discharge intensity in terms of discharge current density, the pulse voltage amplitude is raised to 3.0 kV for considering the voltage drop across the dielectric barriers.[13] It clearly shows that there are two distinct current pulses, which is consistent with the experimental findings.[13,14] The first and second discharge events occur during the rising and falling phases of applied voltage at the time instant of 181 ns and 683 ns, respectively. The amplitude of first discharge current density is 0.20 A/m^2, which is the same as that in Fig. 1(a). The gas voltage obtained by integrating the electric field across the discharge gap is also given in Fig. 1(b), which shows the first peak appears a bit earlier (at 161 ns) than the current density peak (at 181 ns) with the amplitude of 987 V.[16] The higher amplitude of gas voltage than that of the bare electrode case shown in Fig. 1(a) explains that the discharge current density reaches the amplitude within 181 ns, which is much shorter than 600 ns in Fig. 1(a). It is also noted that the time instant of first discharge current density peak at 181 ns is delayed with that of the first gas voltage peak at 161 ns, which is attributed to the quick raising of the gas voltage up to the magnitude higher than the gas breakdown voltage.[5,16] The further falling of gas voltage after the time instant of 181 ns induces the reduction of discharge current density. At the time instant of 200 ns when the applied voltage reaches

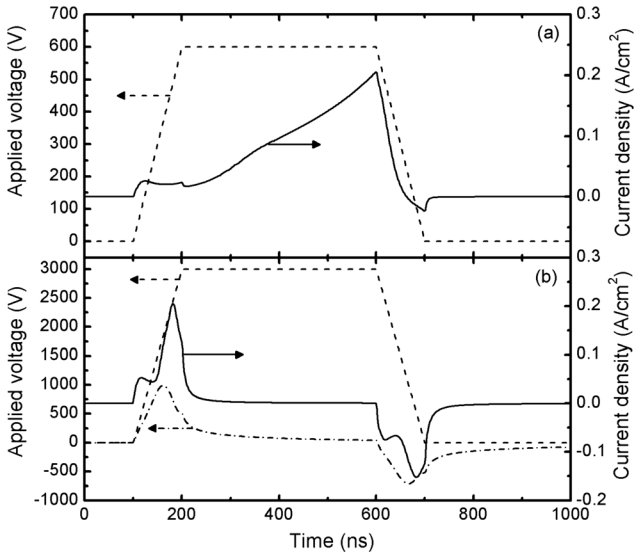

FIG. 1. Waveforms of applied voltage, gas voltage and discharge current density with (a) the bare electrodes and (b) the dielectric barrier electrodes.

the amplitude of 3 kV, the gas voltage reduces to 500 V, whose difference can be compensated by the voltage drop on the dielectric barriers with the space charge accumulation generated in the discharge.[5] The gas voltage keeps going down to 40 V at the time instant of 600 ns, during which the discharge current density approaches zero. With the reduction of applied voltage in the falling phase between 600 ns and 700 ns, the gas voltage is reversed and reaches the amplitude of 712 V at the time instant of 666 ns, which ignites the second discharge event. Again, the second discharge current density peak with the amplitude of 0.15 A/cm^2 (at 683 ns) delays with that of the gas voltage. It also needs to mention the humps in the current density during the voltage rising phase, which are considered to be the displacement current density because of the fact that the discharge gap is mostly capacitive before the gas breakdown and the amplitudes of current density humps grow with the slopes of gas voltage in Fig. 1.[13]

Figure 2 depicts the spatial profiles of electron density, molecular helium ion density and electric field across the interelectrode discharge gap with the bare electrodes at the time instant of 600 ns, corresponding to the discharge current peak in Fig. 1(a). It clearly shows that both the electron and ion density have the bell-shape with the accumulation in the plasma bulk, which is comparable to that in the radio-frequency APGDs with the trapping of plasma species in the plasma bulk.[6] The spatial profile with bell-shape across the discharge gap suggests the high plasma density with electron and ion density of 1.33×10^{12} cm^{-3} and 1.28×10^{12} cm^{-3}, respectively, which is also comparable to that of radio-frequency APGDs and much higher than that of conventional DBD excited with the sinusoidal waveforms.[6,18] At the cathode surface, the space charges induced by the maintenance of ion and exhaustion of electron build up the sheath region, which is also demonstrated by the spatial profile of electric field. The electric field reduces linearly from 48.2 kV/cm at the cathode surface to 2.0 kV/cm at the position of 1.81 mm, which proposes the sheath thickness of around 190 μm.[9]

To reveal the dynamics of discharge with the bare electrodes, the spatio-temporal evolution of electron density and mean electron energy are presented in Figs. 3 and 4, respectively. The electrons are trapped in the middle of discharge gap with the bell-shaped spatial profile when the applied pulse voltage switches off, as shown in Fig. 3 from the time instant of 0 to 100 ns. With growing of the applied voltage,

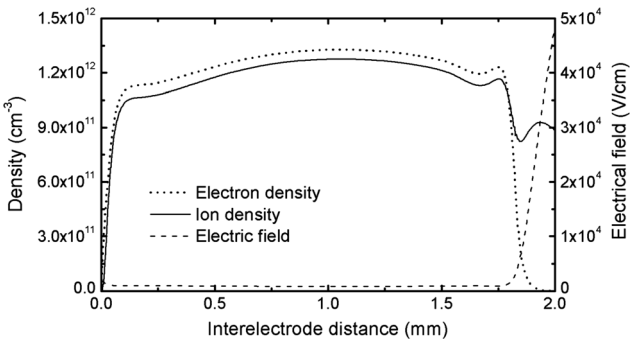

FIG. 2. Spatial profiles of electron density, molecular helium ion density and electric field across the interelectrode discharge gap at the time instant of discharge current peak with the bare electrodes.

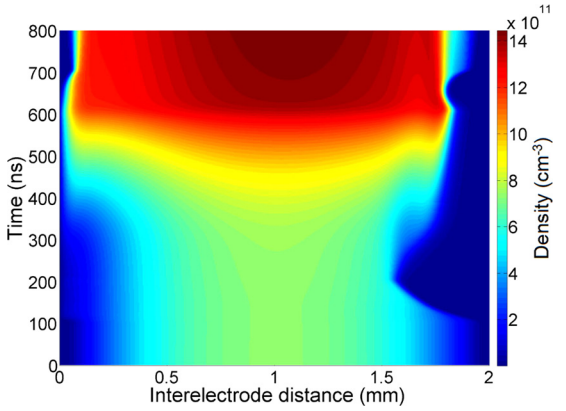

FIG. 3. Spatio-temporal evolution of electron density during the voltage pulse with the bare electrodes.

the electrons are driven by the applied electric field and deplete above the cathode surface until the time instant of 200 ns, during which a sheath forms with the exhaustion of electron. The sheath region can also be recognized in Fig. 4 with the enhanced mean electron energy. Both the spatio-temporal evolution of electron density and mean electron energy indicate that the sheath region expanses with growing of the applied voltage. It suggests that the applied voltage is not high enough for the ignition of electron avalanche,[16] which is confirmed by the spatial profile of electron density in Fig. 3. It is consistent with the explanation of displacement current density hump during the voltage rising phase in Fig. 1. During the voltage amplitude maintaining at 600 V between the time instants of 200 ns and 600 ns, the mean electron energy in the sheath is raised with time, especially in the region close to the cathode, as shown in Fig. 4, which is responsible for the increment of electron density in plasma bulk by ionization, as shown in Fig. 3. Meanwhile, the shrink of sheath region above the cathode is observed both in Figs. 3 and 4, which is due to the electron avalanche and consequently the enhancement of space charges.

The spatial profiles of electron density, molecular helium ion density and electric field across the discharge gap at the time instants of first and second discharge current peaks with the dielectric barrier electrodes are presented in Figs. 5(a) and 5(b), respectively, corresponding to the two

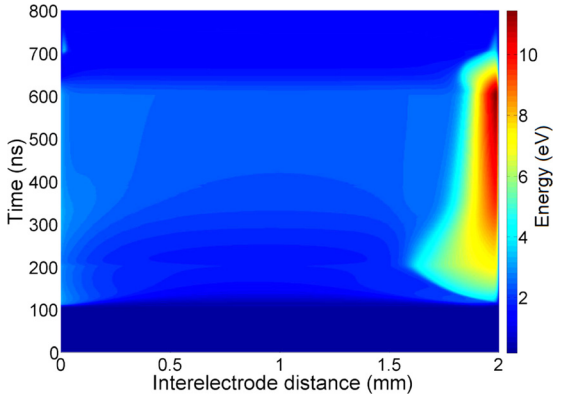

FIG. 4. Spatio-temporal evolution of mean electron energy during the voltage pulse with the bare electrodes.

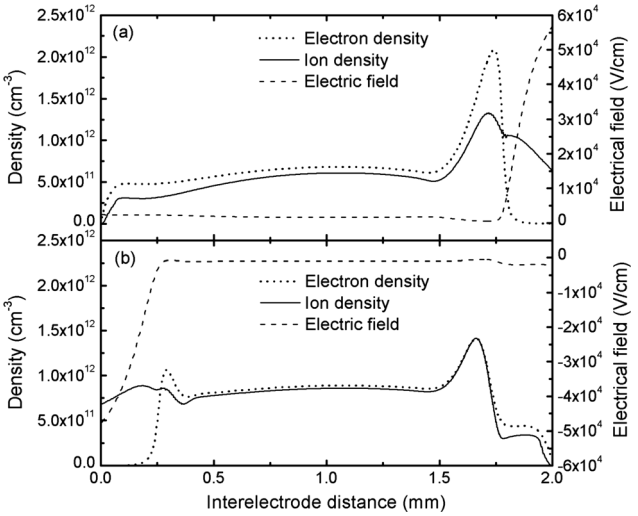

FIG. 5. Spatial profiles of electron density, molecular helium ion density and electric field across the discharge gap at the time instant of (a) the first discharge and (b) the second discharge current peak with the dielectric barrier electrodes.

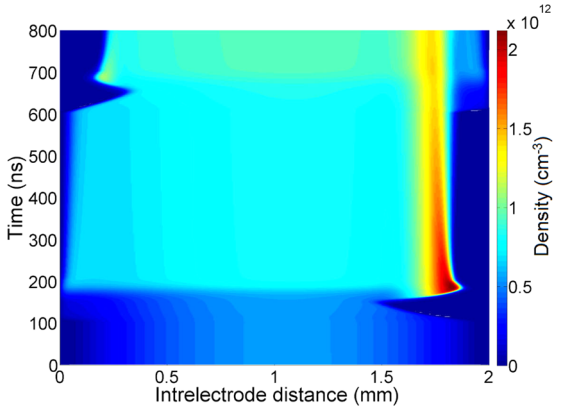

FIG. 6. Spatio-temporal evolution of electron density during the voltage pulse with the dielectric barrier electrodes.

discharge events in Fig. 1(b). The spatial profiles of electron and ion show the localized accumulation in the region between the sheath and plasma bulk, which is different from the bell-shaped spatial profiles with the bare electrodes in Fig. 2. The maximum electron density reaches $2.07 \times 10^{12}\,\mathrm{cm}^{-3}$, as shown in Fig. 5(a), which is about 1.5 times higher than the bare electrode case. The enhancement of electron density can be attributed to the high electric field in the sheath region, which is induced by the elevated applied voltage and gas voltage, as shown in Fig. 1. The electric field of 56.7 kV/cm at the cathode surface, which is higher than that of 48.2 kV/cm in Fig. 2. The sheath thickness of around 230 μm is estimated by the spatial profile of electric field, which is also greater than that of 190 μm in Fig. 2. Both the enhancement of electric field and the expansion of sheath explain the intensified ionization in the region between the sheath and plasma bulk by the energetic electrons traveling through the sheath. On the other hand, the electron density in the plasma bulk is reduced to $6.81 \times 10^{11}\,\mathrm{cm}^{-3}$ at the middle of discharge gap, which is about half magnitude of that of $1.33 \times 10^{12}\,\mathrm{cm}^{-3}$ in Fig. 2.

With changing of the gas voltage polarity shown in Fig. 1(b), the sheath of second discharge is alternatively formed above the other electrode, which acts as the instantaneous cathode, as shown in Fig. 5(b). Given that the temporal interval between the first discharge and second discharge is about 500 ns, the first discharge can maintain until the second discharge ignites, which is demonstrated by the spatial profiles of electron and ion with being localized in the region between the sheath and plasma bulk. According to the amplitude of gas voltage in Fig. 1(b), the electric field at the instantaneous cathode is reduced to 47.6 kV/cm, which indicates the low mean electron energy and ionization event in the region between the sheath and plasma bulk, as demonstrated by the spatial profile of electron density. On the other hand, the electron density at the middle of discharge gap is enhanced to be $8.87 \times 10^{11}\,\mathrm{cm}^{-3}$. The sheath thickness is estimated to be 257 μm, which is increased because of the weakening of space charge in the sheath region, compared with that of the first discharge.

The spatial non-uniformity of plasma density has been shown in terms of electron density at the time instants of discharge current peaks in Fig. 5. The spatio-temporal evolution of the electron density is illustrated in Fig. 6. By applying the voltage, the electrons are depleted above the cathode surface and consequently the sheath region is formed, which is similar to that of the discharge with the bare electrodes shown in Fig. 3. With the shrinking of sheath region and strengthening of sheath electric field, the first discharge is ignited with intensified electron density in the region between the sheath and plasma bulk. The discharge is maintained afterwards until the second discharge takes place (at 600 ns) with the sheath formed above the other electrode (the left electrode in Fig. 6). It shows that the electron density in the region between the sheath and plasma bulk of the second discharge is much weaker than that of the first discharge and the electron density in the plasma bulk is enhanced, which are consistent with that in Fig. 5.

Figure 7 demonstrates the spatio-temporal evolution of mean electron energy during the voltage pulse with the dielectric barrier electrodes. The sheath region can be recognized with the elevated mean electron energy, which demonstrates the sheath dynamics during the discharge pulse with the expansion and shrinking of the sheath region. There are two sheath regions formed above the instantaneous cathode, whose profiles are

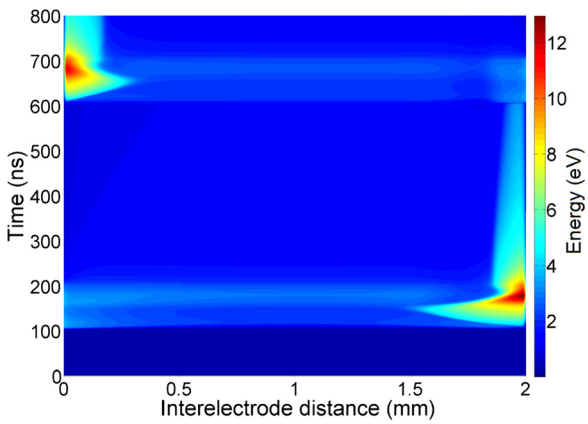

FIG. 7. Spatio-temporal evolution of mean electron energy during the voltage pulse with the dielectric barrier electrodes.

corresponding to the depletion region of electron, as shown in Fig. 6. It also indicates that the magnitude of mean electron energy reaches about 12 eV during the first discharge, which is higher than that of the second discharge. It suggests the first discharge has higher discharge intensity than the second discharge in terms of electron density and discharge current density.

IV. SUMMARY

The characteristics and mechanism of pulsed atmospheric pressure glow discharges with and without dielectric barriers are studied by one-dimensional numerical simulation. It is found that the amplitude of applied pulse voltage has to be raised significantly by introducing the dielectric barriers to achieve the same discharge intensity in terms of discharge current density. One discharge event is ignited gradually during the voltage pulse with the bare electrodes and the generated discharge is uniformly distributed across the discharge gap, especially in the plasma bulk. On the other hand, two discharge events happen during the rising and falling phases of voltage pulse, respectively, with the dielectric barrier electrodes. The elevated gas voltage enhances the electric field and mean electron energy in the sheath region, which induces the abrupt discharge ignition and the subsequent electron accumulation in the region between the sheath and plasma bulk.

ACKNOWLEDGMENTS

This work was funded by the Natural Science Foundation of China (Grant Nos. 10835004 and 10905010) and sponsored by Shanghai Shuguang Program (Grant No. 08SG31) and the Fundamental Research Funds for the Central Universities.

[1]J. R. Roth, S. Nourgostar, and T. A. Bonds, IEEE Trans. Plasma Sci. **35**, 233 (2007).
[2]S. Y. Moon, J. W. Han, and W. Choe, Thin Solid Films **506**, 355 (2006).
[3]J. Zhang, Y. Guo, J. Z. Xu, X. S. Fang, H. K. Xie, D. L. Shi, P. He, and W. J. van Ooij, Appl. Phys. Lett. **86**, 131501 (2005).
[4]B. Gweon, M. Kim, D. B. Kim, D. Kim, H. Kim, H. Jung, J. H. Shin, and W. Choe, Appl. Phys. Lett. **99**, 063701 (2011).
[5]F. Massines, A. Rabehi, P. Decomps, R. B. Gadri, P. Segur, and C. Mayoux, J. Appl. Phys. **83**, 2950 (1998).
[6]J. J. Shi and M. G. Kong, Appl. Phys. Lett. **90**, 101502 (2007).
[7]T. Martens, A. Bogaerts, and J. V. Dijk, Appl. Phys. Lett. **96**, 131503 (2010).
[8]J. L. Walsh and M. G. Kong, Appl. Phys. Lett. **88**, 171501 (2006).
[9]T. Ito, T. Kanazawa, and S. Hamaguchi, Phys. Rev. Lett. **107**, 065002 (2011).
[10]T. Shao, C. Zhang, K. H. Long, D. D. Zhang, J. Wang, P. Yan, and Y. X. Zhou, Appl. Surf. Sci. **256**, 3888 (2010).
[11]E. Noriega, G. Shama, A. Laca, M. Diaz, and M. G. Kong, Food Microbiol. **28**, 1293 (2011).
[12]N. Y. Cui and N. M. D. Brown, Appl. Surf. Sci. **189**, 31 (2002).
[13]X. J. Huang, L. Q. Sun, Y. Bao, J. Zhang, and J. J. Shi, Phys. Plasmas **18**, 033503 (2011).
[14]X. P. Lu and M. Laroussi, J. Phys. D: Appl. Phys. **39**, 1127 (2006).
[15]J. Zhang, Y. H. Wang, and D. Z. Wang, Thin Solid Films **519**, 7020 (2011).
[16]F. Iza, J. L. Walsh, and M. G. Kong, IEEE Trans. Plasma Sci. **37**, 1289 (2009).
[17]G. J. M. Hagelaar and L. C. Pitchford, Plasma Sources Sci. Technol. **14**, 722 (2005).
[18]M. Moravej, X. Yang, R. F. Hicks, J. Penelon, and S. E. Babayan, J. Appl. Phys. **99**, 093305 (2006).